Proton MR spectroscopy of pediatric cerebellar tumors.

Z Wang, L N Sutton, A Cnaan, J C Haselgrove, L B Rorke, H Zhao, L T Bilaniuk and R A Zimmerman

AJNR Am J Neuroradiol 1995, 16 (9) 1821-1833
http://www.ajnr.org/content/16/9/1821

Proton MR Spectroscopy of Pediatric Cerebellar Tumors

Zhiyue Wang, Leslie N. Sutton, Avital Cnaan, John C. Haselgrove, Lucy B. Rorke, Huaqing Zhao, Larissa T. Bilaniuk, and Robert A. Zimmerman

PURPOSE: To investigate the role of proton MR spectroscopy in pediatric cerebellar tumor diagnosis. **METHODS:** Single voxel pulse sequences with long echo time (135 or 270 milliseconds, voxel size 8 to 19 cm^3), were used to obtain proton spectra of primary pediatric cerebellar tumors. Eleven primitive neuroectodermal tumors (patient age, 2 to 12 years; mean, 7 years), 11 low-grade astrocytomas (age, 2 to 16 years; mean, 9 years), 4 ependymomas (age, 1 to 6 years; mean, 4 years), 1 mixed glioma ependymo-astrocytoma (age, 11 years), 1 anaplastic ependymoma (age, 7 years), 1 ganglioglioma (age, 14 years), and 1 malignant teratoma (age, 6 days) were studied. Control cerebellum spectra were acquired from five patients without abnormality in cerebellum (age, 2 to 15 years; mean, 8 years). The signal intensities from choline-containing compounds (Cho), creatine/phosphocreatine (Cr), *N*-acetyl-aspartate (NAA), and lactate (Lac) were quantified. The mean and standard deviation of metabolite ratios were calculated. **RESULTS:** The control spectra ratios (NAA:Cho = 1.49 ± 0.36, Cr:Cho = 1.13 ± 0.23) were distinct from the tumor spectra (NAA:Cho = 0.41 ± 0.27 and Cr:Cho = 0.37 ± 0.23). Most of primitive neuroectodermal tumors had low NAA:Cho (0.17 ± 0.09) and Cr:Cho (0.32 ± 0.19). Compared with primitive neuroectodermal tumors, low-grade astrocytomas and ependymomas had higher NAA:Cho ratio (0.63 ± 0.19 and 0.39 ± 0.12). The Cr:Cho ratio was higher for ependymomas (0.60 ± 0.20) than for astrocytomas (0.27 ± 0.12) and primitive neuroectodermal tumors. No NAA was found in the malignant teratoma. Lac:Cho ratio was 0.66 ± 0.40, 0.58 ± 0.30, and 0.08 ± 0.12 for astrocytoma, ependymoma, and primitive neuroectodermal tumor, respectively. Lactate was elevated in the mixed glioma ependymo-astrocytoma, ganglioglioma, and teratoma. The NAA and lactate signals were sometimes obscured by lipids in the spectra. Discriminant analysis was carried out using NAA:Cho and Cr:Cho ratios to differentiate the three major tumor types. The sensitivity/specificity values for diagnosing astrocytoma, ependymoma, and primitive neuroectodermal tumor were found to be 0.91/0.84, 0.75/0.92, and 0.82/0.89, respectively, based on this study. **CONCLUSION:** In many cases, proton MR spectroscopy can be used to help differentiate cerebellar primitive neuroectodermal tumor, low-grade astrocytoma, and ependymoma.

Index terms: Magnetic resonance, spectroscopy; Cerebellum, neoplasms; Children, neoplasms

AJNR Am J Neuroradiol 16:1821–1833, October 1995

Correct initial diagnosis of brain tumor type and grade before a surgical procedure would improve treatment and reduce risks to the patients. In many cases, the information obtained from magnetic resonance (MR) imaging and computed tomography (CT) is able to give a correct diagnosis of tumor type and whether it is benign or malignant (1). This is based on the location, size, and extent of the tumor; enhancement characteristics with contrast agents as well as with T1 and T2 relaxation properties of the tumor tissue; and whether the tumor contains cystic, necrotic, calcific, or hemorrhagic components. Despite many successes of diagnostic imaging, there are always exceptions. Sometimes a common tumor has an atypical appearance on MR images. Certain rare tumors may mimic the appearance of more common

Received November 18, 1994; accepted after revision May 11, 1995.

From the Departments of Radiology (Z. W., J. C. H., L. T. B., R. A. Z.), and Neurosurgery (L. N. S.), Division of Biostatistics and Epidemiology (A. C., H. Z.), and the Department of Pathology (L. B. R.), The Children's Hospital of Philadelphia (Pa).

Address reprint requests to Robert A. Zimmerman, MD, MRI Unit, Department of Radiology, The Children's Hospital of Philadelphia, 324 S 34th St, Philadelphia, PA 19104-4345.

AJNR 16:1821–1833, Oct 1995 0195-6108/95/1609–1821

tumors. MR spectroscopy provides a unique modality with which to study in vivo tumor metabolism noninvasively (2). In vivo spectroscopy studies of human brain tumors have been an active area of research (3–43). Pediatric brain tumors are distinct from those of adults, and many different tumor types are encountered in clinical practice. The metabolic information obtained from MR spectroscopy can be used to complement MR imaging and CT as an additional predictor of tumor aggressiveness. In situations in which CT and MR imaging cannot give definite diagnosis, MR spectroscopy can be helpful by providing information that would separate tumors according to categories of malignancy (36). This information, when combined with imaging, helps to establish a better diagnosis of the likely tumor pathology. Presently, the clinical utility of MR spectroscopy in tumor diagnosis before surgical operation has not been fully explored. Recently, it has been reported that in vivo proton MR spectroscopy is able to differentiate five types of the most common adult supratentorial brain tumors (Preul MC et al, the Society of Magnetic Resonance "Linear Discriminant Analysis Based on Proton MR Spectroscopic Imaging of Human Brain Tumors Improves Pre-operative Diagnosis," proceedings of the Society of Magnetic Resonance Second Annual Meeting, August 6–12, 1994, p 125). In an earlier paper, MR spectroscopy studies on 25 cases of pediatric brain tumors that occurred at all locations in the brain were reported (36). In this paper, we investigate whether MR spectroscopy is helpful in differentiating major types of pediatric cerebellar tumors.

Materials and Methods

Patients

This MR spectroscopy study was carried out between January 1990 and March 1995. The patient eligibility criteria were: (*a*) the patient had a newly diagnosed primary cerebellar tumor with a size larger than 10 cm^3 and had not received surgery or therapy; and (*b*) the patient was medically stable and able to undergo the MR imaging and spectroscopy examination. MR spectroscopy was performed in the same session as the clinically indicated routine MR imaging. All tumor patients underwent surgery or biopsy shortly after the MR studies, so that a pathologic diagnosis was available from resected tumor tissue. Patients younger than 10 years of age were sedated with either pentobarbital (older than 18 months) or chloral hydrate (younger than 18 months) to obtain motion-free MR studies over a span of 1.5 hours. For older children, no sedation was used. Informed consent for the MR spectroscopy was obtained from the parents or guardians of the patients. Control cerebellum spectra were measured from patients without any cerebellar abnormalities who were undergoing MR imaging for other disorders.

MR Spectroscopy

All studies were performed on a 1.5-T Siemens Magnetom SP MR scanner at the MR imaging unit. A circular polarized head coil was used for all studies. MR spectroscopy was performed after routine MR imaging. Localized water-suppressed proton MR spectra were obtained with either stimulated echo acquisition mode (STEAM) sequence (44) with the middle interval 30 milliseconds and an echo time of 270 milliseconds, or spin-echo (also called point-resolved spectroscopy [PRESS]) sequence (45) with an echo time of 135 milliseconds. When this investigation began, STEAM with long echo times (135 or 270 milliseconds) were the only sequences installed on the scanner. STEAM with an echo time of 270 milliseconds was chosen over STEAM with an echo time of 135 milliseconds to avoid the multiquantum effects on the lactate signal. Later, spin-echo sequences became available, which provided a twofold improvement in signal sensitivity over STEAM, and a spin-echo sequence with echo time of 135 milliseconds was used. Repetition time of 1.5 seconds was used for these studies using STEAM and spin echo. The sampling volumes were 8 to 19 cm^3. The selection of the region of interest was guided by the MR images. The criteria for the region of interest selection were to maximize sampling volume while minimizing inclusion of normal brain tissue surrounding the tumor and any cysts inside the tumor. Typically, 200 to 300 scans were averaged for each sampling volume. Reference scans without water suppression also were collected for correcting eddy current effects (46). From June 1992 to November 1993, we participated in the multicenter clinical trial organized by Siemens (Negendank WG et al, "Single-Volume Proton MR Spectroscopy in Patients with Primary Brain Tumors: A Multicenter Study," Radiological Society of North America 1993 scientific program, p 297). All measurements then were performed with a standard protocol using a spin-echo sequence with 1600/135/256 (repetition time/echo time/excitations) and volume of interest of 2^3 cm^3. All data reported here were collected before injection of a paramagnetic contrast agent.

Major components found in the proton MR spectra were $(CH_3)_3$ group of choline-containing compounds (Cho) at 3.2 ppm, CH_3 group of creatine and phosphocreatine (Cr) at 3.0 ppm, CH_3 group of *N*-acetyl-aspartate (NAA) at 2.0 ppm, and a doublet attributable to CH_3 of lactate (Lac) at 1.31 ppm (47). Sometimes a doublet at 1.45 ppm attributable to CH_3 of alanine also can be detected in brain tumors. The peak assignments here did not rule out possibilities that other metabolites were contained in these peaks. Sometimes lipid signals also were present in the spectra. The lipid signals were in the 1- to 2-ppm range. A

peak was assigned to be lactate if its position, phase, and linewidth were consistent with lactate. The center of the peak should be at 1.31 ppm; lactate signal should have a negative sign relative to other signals if echo time is 135 milliseconds, and a positive sign if echo time is 270 milliseconds; the width of the signal should be roughly 0.2 ppm, corresponding to a doublet with 7 Hz splitting. For some cases, the lactate had a clear doublet appearance, whereas in other cases the splitting was not clear. For some cases, it was not possible to determine how much lactate was present or whether it was present at all owing to the presence of lipid signals. The lipid signals came from either fatty tissue adjacent to the region of interest or the tumor tissue inside the region of interest.

Data processing of the MR spectroscopy was performed in several steps. These consisted of eddy current correction (46), apodization (48) of corrected time domain signal by multiplying a Gaussian function to enhance the signal-to-noise ratio, Fourier transform to the frequency domain, phase correction, and peak area calculation of the absorption spectrum. Although both Lorentzian and Gaussian functions are frequently used for apodization, we prefer to use a Gaussian function because the tails of the resulting peak are smaller. The peak area is a measure of the number of the nuclear spins in the sampling volume, subject to relaxation effects. The area of the peak is not affected by apodization. Sometimes the baseline of the absorption spectrum also was adjusted by manually choosing a number of zero points, when water suppression was not satisfactory for technical reasons. For most cases, the lines were well resolved. The area of each peak was evaluated with system software by direct integration of the Gaussian broadened spectrum over a frequency interval. In calculating the areas of choline and creatine, we assumed that signal above 3.1 ppm comes from choline and below 3.1 ppm was assigned to creatine. When the peaks overlap, this procedure overestimates the signal contribution from the smaller peak. Because of their short T2 values, the amount of lipids was much less on the long echo spectra. For cases in which lactate is obscured by lipids, upper limits of the lactate levels were estimated. The lactate levels in these patients were excluded from statistical analysis. The linewidth of the lactate doublet was assumed to be 0.2 ppm, and the upper limit of the peak height was assumed to be the maximum signal intensity in the range 1.1 to 1.5 ppm. The upper limit of the lactate level was estimated as the linewidth multiplied by the peak height.

To evaluate the limit of precision of the measurement, the lower bound of the standard error of peak area attributable to random noise was calculated. The ultimate uncertainties of the measurement were limited by the Cramer-Rao lower bounds (49). However, this lower bound can be reached only by a weighted least squares fit on apodized spectra. Recently, we have developed a method (Z. Wang and J. Haselgrove, "Determinations of Errors in MR Spectroscopy Measurement Caused by Random Noise," proceedings of the Society of Magnetic Resonance Third Scientific Meeting and European Society for Magnetic Resonance in Medicine and Biology 12th Annual Meeting, August 19–25, 1995, Nice, France, p 1949) to calculate the uncertainties of peak area obtained by any analysis algorithm. This method can be used for both independent and correlated noise. We have tested this method by using Monte Carlo simulations, and excellent agreement was obtained. This method is used to estimate limits in precision of peak areas, assuming each peak is a Gaussian.

Statistical Methods

Extended Fisher's Exact Test (50) was used to examine whether there was an association between tumor type and patient sex. Analysis of variance (ANOVA) was used to examine whether there was a relation between tumor type and patient age. *T* tests were used to examine whether metabolic ratios within the same tumor group were different by pulse sequence. ANOVA was used to test whether the metabolite ratios were different for the tumor types and the control group, and pairwise comparisons using a Bonferroni correction were done. For the three major tumor types, all variables that were significantly associated with tumor type were entered into a discriminant analysis (51). Discriminant analysis enables the user to define regions based on the metabolite ratios and other possible predicting variables, so that a tumor with values in one specific region is likely to belong to a specific type. The underlying algorithm assigns the region based on a Mahalanobis distance, which is a generalized distance measure. Analysis was done using SPSS for Windows (SPSS Inc, Chicago, Ill). Based on the results, a decision rule was constructed that defined regions corresponding to tumor types, and patients were classified by it. Sensitivity, specificity, positive predictive ability, and negative predictive ability were calculated based on the classification.

Results

We performed MR spectroscopy on 41 patients with cerebellar tumors using STEAM with an echo time of 270 milliseconds, and spin-echo with an echo time of 135 milliseconds. Two sedated patients woke up during the study, so the examination could not be finished. Among the 39 patients who had complete MR spectroscopy study, spectra from 4 patients were excluded because of poor quality. In 1 of the remaining 35 cases, the tumor was too small to fill a 8 cm^3 region of interest, and the spectrum was contaminated by normal surrounding tissue. In a second case, the tumor was mainly cystic, and the spectrum from the solid tumor portion could not be obtained. In a third case, the linewidth of the 2.0-ppm peak was excessively wide (about 0.3 ppm) despite narrow choline and creatine linewidths (about

TABLE 1: Tumor types and ages of patients in whom spectra of satisfactory quality were obtained

Tumor Type	Number of Patients	Age, mean (range)
Astrocytoma	11	9 (2–16) y
Ependymoma	4	4 (1–6) y
Primitive neuroectodermal tumor	11	7 (2–12) y
Ependymo-astrocytoma	1	11 y
Anaplastic ependymoma	1	7 y
Ganglioglioma	1	14 y
Teratoma	1	6 d
Control	5	8 (2–15) y

0.1 ppm). The peak height was about half that of the choline. It was likely that the broad 2-ppm peak contained large amount of lipids (52). For this case, NAA level could not be determined. These three spectra also were rejected. We also excluded two studies performed after gadopentetate dimeglumine injection. The distribution of age and tumor type of the remaining 30 patients, 20 male and 10 female, is listed in Table 1. Five control cerebellum spectra also were acquired from patients without cerebellar abnormalities.

Because absolute concentrations were not calibrated, only ratios among different metabolites were obtained. Because choline signal was always nonzero, the results were presented as ratios to choline. The baseline correction procedure unavoidably introduced certain errors, especially on the weak signals and broad components. For major peaks including choline, creatine/phosphorus creatine, and NAA, these uncertainties were not substantial. The uncertainties attributable to random noise in choline peak area were typically 3% to 5% for primitive neuroectodermal tumor, 10% to 20% for ependymoma and astrocytoma, and 7% for normal tissue. For some cases, lactate could not be quantified because of lipid contamination. Upper limits of lactate levels were estimated for these cases but were excluded from statistical analysis. For approximately half of the cases reported in this paper the voxels were well within the tumor boundaries. For about one third of the cases, the region of interest contained 5% or less of normal tissue. For the remaining cases, the tumor tightly fit into the region of interest without normal tissue contamination.

Table 2 gives average values and standard deviations of metabolite ratios for spectra obtained with each pulse sequence within tumor subgroups and control. For subgroups with fewer than four members, the standard deviation is not given, because it cannot be estimated meaningfully with a very small sampling size.

TABLE 2: Tumor in vivo MR spectroscopy results*

Tissue Type	Sequence†	Number of Spectra Obtained	NAA:Cho	Cr:Cho	Lac:Cho
Control	SE_135	3	1.59	1.15	0.00 (n = 2)‡
	ST_270	2	1.33	1.09	0.13
	overall	5	1.49 (0.36)	1.13 (0.23)	0.07 (0.09) (n = 4)‡
Astrocytoma	SE_135	7	0.62 (0.22)	0.23 (0.10)	0.49 (0.31) (n = 4)‡
	ST_270	4	0.65 (0.18)	0.34 (0.13)	0.83 (0.45)
	overall	11	0.63 (0.19)	0.27 (0.12)	0.66 (0.40) (0 = 8)‡
Ependymoma	SE_135	1	0.30	0.68	0.63
	ST_270	3	0.42	0.57	0.57
	overall	4	0.39 (0.12)	0.60 (0.20)	0.58 (0.30)
Primitive neuroectodermal tumor	SE_135	7	0.16 (0.07)	0.30 (0.21)	0.01 (0.02) (n = 5) ‡
	ST_270	4	0.18 (0.13)	0.35 (0.15)	0.21 (n = 3)‡
	overall	11	0.17 (0.09)	0.32 (0.19)	0.08 (0.12)
Ependymo-astrocytoma	SE_135	1	0.84	0.25	0.25
Anaplastic ependymoma	SE_135	1	0.47	0.22	. . .‡
Ganglioglioma	ST_270	1	0.70	1.03	0.36
Teratoma	ST_270	1	0.00	0.61	1.08
All Tumors	SE_135	17	0.42 (0.28)	0.29 (0.18)	0.26 (0.31) (n = 11)‡
	ST_270	13	0.41 (0.27)	0.47 (0.25)	0.59 (0.41) (n = 12)‡
	overall	30	0.41 (0.27)	0.37 (0.23)	0.43 (0.39) (n = 23)‡

* The values listed are means and standard deviations of ratios of the metabolite peak areas.

†SE_135 indicates spin-echo sequence with an echo time of 135 milliseconds and ST_270 indicates STEAM sequence with an echo time of 270 milliseconds.

‡ Lactate could not be quantified because of lipids contamination in some cases.

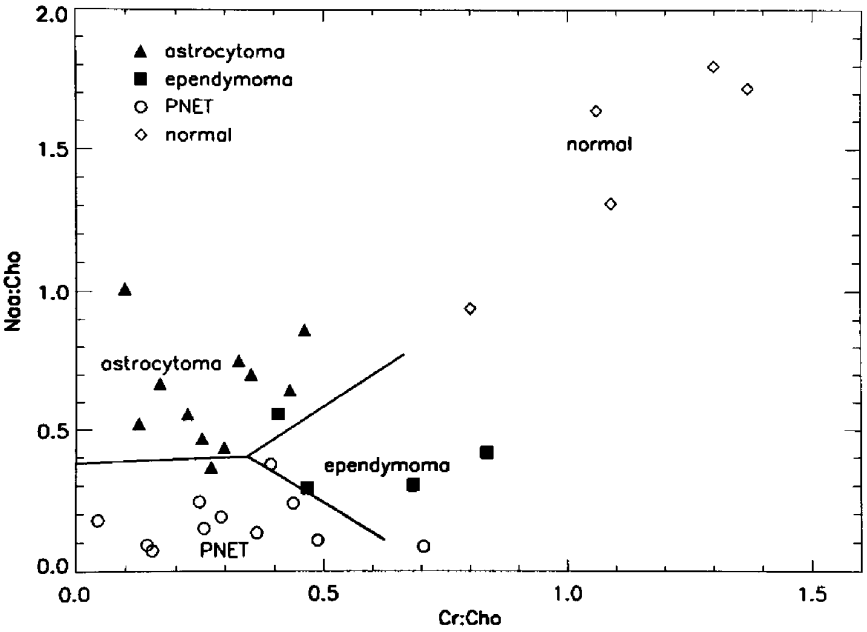

Fig 1. NAA:Cho versus Cr:Cho scattergram for astrocytoma, ependymoma, primitive neuroectodermal tumor (*PNET*), and normal cerebellar tissue. The straight lines are boundaries between the three tumor types found by discriminant analysis.

There were no significant differences based on echo time, by a *t* test, thus we used the overall means in all subsequent analysis. Because of the presence of lipid in some spectra, lactate quantitation was available only for a fraction of patients. For those cases in which lactate was not quantified, the estimated upper limit of Lac:Cho ranges from 0.2 to 0.5. The number of spectra within each row for which lactate was quantified is given in parentheses. The results also are presented by Cr:Cho versus NAA:Cho scattergram for the three major tumor types and control (Fig 1).

Control Spectra

Two control spectra were acquired with STEAM with an echo time of 270 milliseconds and three control spectra were acquired with spin-echo with an echo time of 135 milliseconds. A control cerebellum spectrum is shown in Figure 2. There is no overlap between the control spectra and the tumor spectra. Our experience indicates that control spectra acquired from cerebellum are different from those in the supratentorial brain tissues, with lower NAA:Cho ratio. This is consistent with the literature (47).

Low-Grade Astrocytoma

Eleven patients studied were diagnosed by microscopic pathologic examinations to have histologically benign astrocytoma. Figure 3 shows the MR imaging and spectroscopy of a cerebellar astrocytoma. Both Cr:Cho and NAA:Cho ratios were decreased compared with normal brain tissue. Eight astrocytomas had elevated signals at 1.31 ppm, which were assigned to lactate. The lactate was increased to various levels. In the other three spectra, all obtained with the spin-echo 135 echo time sequence, lactate levels may be elevated but could not be determined because of increased lipid signal. In one case of elevated lipids, the tumor recurred after surgery, indicating a more aggressive tumor than other low-grade astrocytomas studied

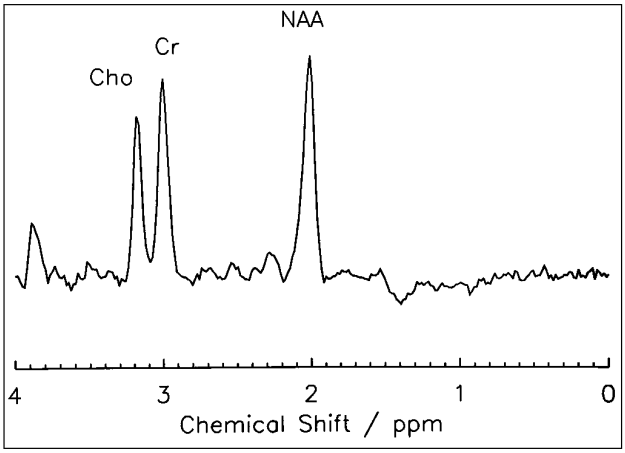

Fig 2. A control cerebellum spectrum obtained with a spin-echo sequence (1600/135/256) and a voxel size of $2 \times 2 \times 2$ cm^3.

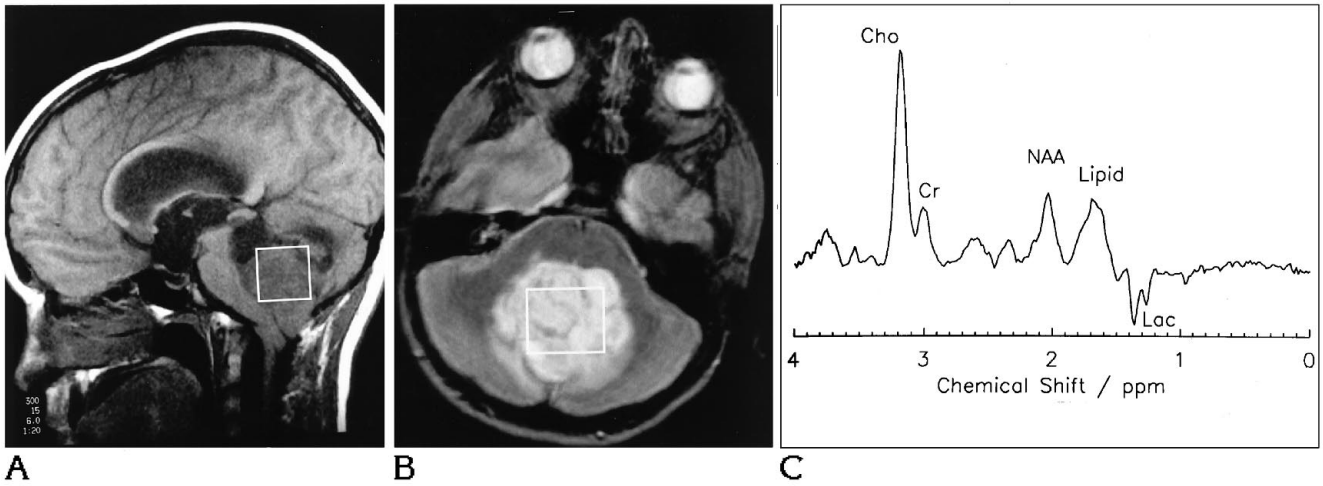

Fig 3. MR imaging and spectroscopy of a cerebellar astrocytoma. The MR spectroscopy sampling volume is indicated in A and B by boxes.

A, T1-weighted sagittal MR image.

B, T2-weighted transverse MR image.

C, The tumor MR spectrum. The spectrum was obtained with a spin-echo sequence (1500/135/200) with voxel size of $3 \times 2.5 \times 2.5$ cm^3.

here. Alanine was seen in some spectra, together with high levels of lactate.

Ependymoma

Three patients studied using STEAM with an echo time of 270 milliseconds and one patient studied using spin-echo with an echo time of 135 milliseconds were found to have an ependymoma. Figure 4 shows a case of ependymoma. Large signals at 1.3 ppm were observed in all four patients. The peak was negative for the spin-echo 135 echo time spectrum. These signals were assigned as lactate. The NAA:Cho and Lac:Cho values for ependymoma and astrocytoma were similar. However, ependymomas had a higher average Cr:Cho levels then astrocytomas.

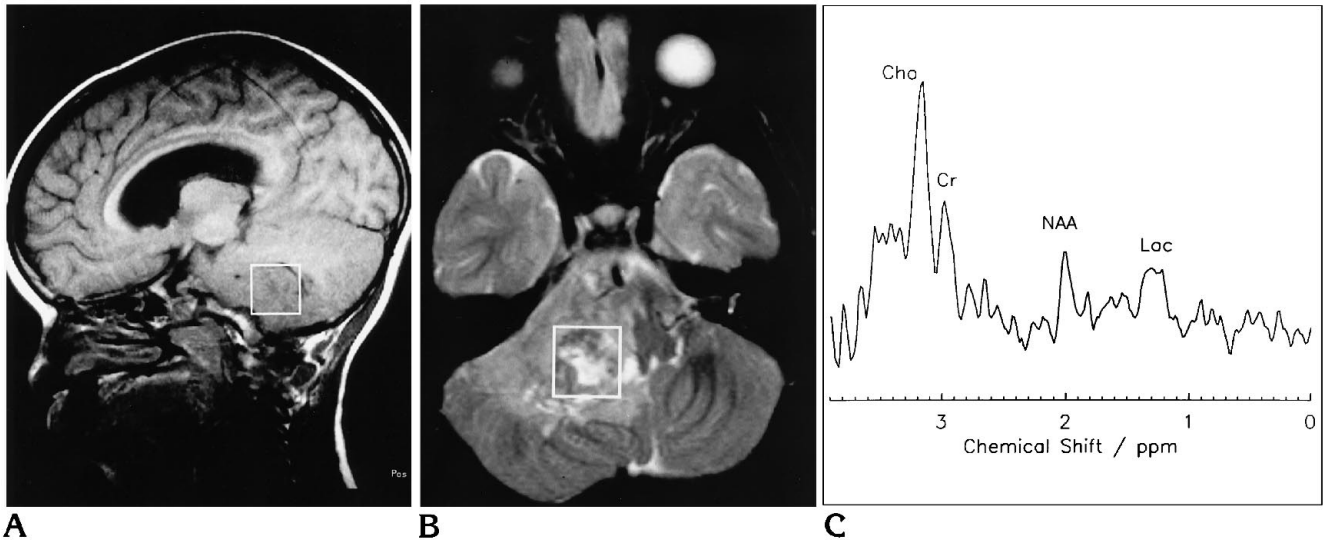

Fig 4. MR imaging and spectroscopy of an ependymoma. The MR spectroscopy sampling volume is indicated in A and B by boxes.

A, T1-weighted sagittal MR image.

B, T2-weighted transverse MR image.

C, The tumor spectrum. The spectrum was obtained with a STEAM sequence (1500/270/400) with voxel size of $2 \times 2 \times 2$ cm^3.

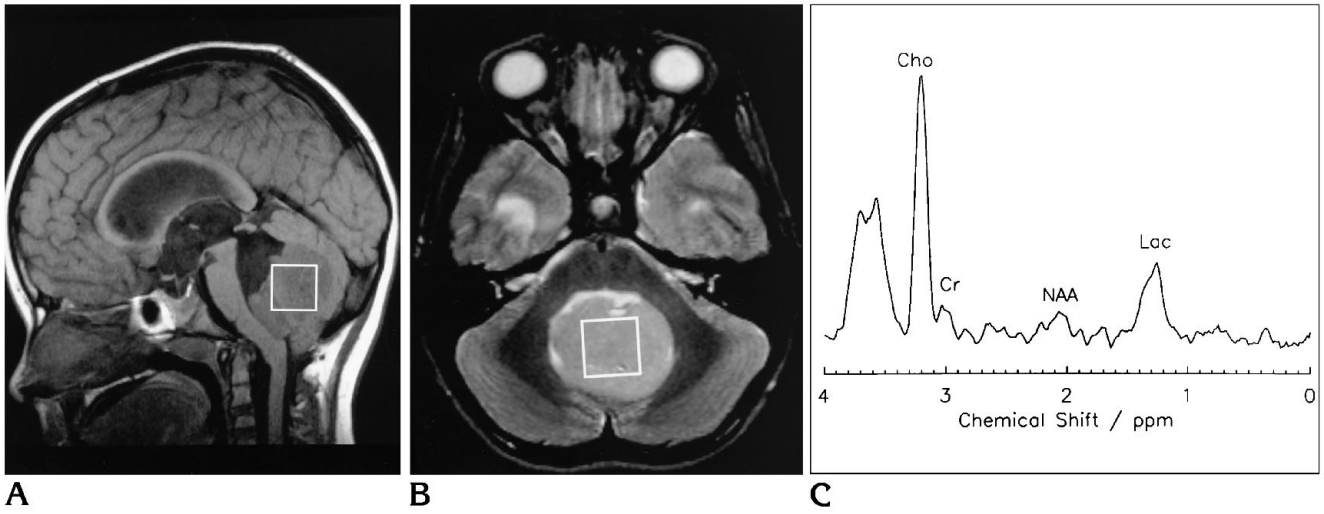

Fig 5. MR imaging and spectroscopy of a primitive neuroectodermal tumor. The MR spectroscopy sampling volume is indicated in A and B by boxes.

A, T1-weighted sagittal MR image.

B, T2-weighted transverse MR image.

C, The tumor spectrum. The spectrum was obtained with a STEAM sequence (1500/270/256) with voxel size of $2 \times 2 \times 2$ cm^3.

Primitive Neuroectodermal Tumors

Eleven primitive neuroectodermal tumor patients were studied. Cr:Cho and NAA:Cho ratios were low in most primitive neuroectodermal tumors. Most primitive neuroectodermal tumors did not have highly elevated Lac:Cho ratios, and in many cases lactate was not detectable. However, peaks presumably attributable to lipids or other unknown metabolites showed up frequently at various positions from 1 to 2 ppm in the spectra. Figure 5 shows the MR imaging and spectroscopy of a primitive neuroectodermal tumor patient with a vermian tumor.

Other Cerebellar Tumors

Other tumors studied included one case each of mixed glioma ependymo-astrocytoma, anaplastic ependymoma, ganglioglioma, and malignant teratoma. Ganglioglioma is a tumor of neuronal and glial cells. The NAA:Cho and Cr:Cho for the mixed glioma ependymo-astrocytoma and the anaplastic ependymoma were similar to that for other astrocytomas. Teratoma is a type of a germ cell tumor. For the case of malignant teratoma, no NAA was observed, and the lactate was elevated. The teratoma would fall into the region of primitive neuroectodermal tumor in the NAA:Cho versus Cr:Cho scattergram. The ganglioglioma had higher NAA:Cho and Cr:Cho values relative to other tumors. Lactate was elevated.

Discriminant Models

Using extended Fisher's Exact Test and ANOVA, it was found that sex, pulse sequence, and age were not associated with pathologically determined tumor type. Therefore, only metabolite ratios were considered for the discriminant analysis. Because the range of ratios for the control group was totally separated from the range for the patients with tumors, no further analysis that included the controls was necessary. Three ANOVA models for NAA:Cho, Cr:Cho, and Lac:Cho were fit to examine overall differences in these ratios between the tumor groups and gave $P < .00005$, $P = .0074$, and $P = .0028$ for the respective ratios. Pairwise comparisons with Bonferroni corrections on NAA:Cho showed that astrocytomas were significantly different from ependymomas ($P = .029$) and primitive neuroectodermal tumors with $P < .0005$. Ependymomas were marginally different from primitive neuroectodermal tumors, with $P = .05$. However, for Cr:Cho there was no significant difference between astrocytomas and primitive neuroectodermal tumors, and both were significantly different from ependymomas, with $P = .007$ and $P = .022$, respectively. Finally, for Lac:Cho, there was no difference between astrocytoma and ependymomas, and both were different from primitive neuroectodermal tumors, with $P = .003$ and $P = .041$, respectively.

TABLE 3: Classification results of the discriminant analysis on the three major tumor types using NAA:Cho and Cr:Cho as discriminant variables

Actual Tumor Type	Number of Cases	Predicted Tumor Type		
		Astrocytoma	Ependymoma	Primitive Neuoectodermal Tumor
Astrocytoma	11	10	0	1
Ependymoma	4	1	3	0
Primitive neuroectodermal tumor	11	0	2	9

Three types of tumors (astrocytoma, ependymoma, and primitive neuroectodermal tumor) were analyzed using discriminant analysis. We did not include the other four tumor types, because we had only one of each tumor. The main discriminant analysis used NAA:Cho and Cr:Cho as discriminant variables. The discriminant analysis (SPSS for Windows) yielded the boundaries of deciding how to classify a patient into a tumor group based on NAA:Cho and Cr:Cho values. These boundaries are plotted in Figure 1 as solid straight lines. The dividing lines were based on an assumption of equal covariance matrices, which was tested using Box's *M* test and found acceptable. Table 3 gives classification results of this analysis. Four (15%) of the 26 patients would have been incorrectly classified.

Table 4 summarizes the sensitivity, specificity, positive predictive value, and negative predictive value for the three tumor types based on the classification scheme of Figure 1. The classification results for the three major tumor types are based on Table 3. In calculating values in Table 4, all 30 tumors in Table 1 are included. Based on Figure 1 and Table 2, we find that: (*a*) the mixed glioependymoastrocytoma and the anaplastic ependymoma would have been misclassified as astrocytoma; (*b*) the MR spectroscopy would have misclassified the malignant teratoma as primitive neuroectodermal tumor; (*c*) the ganglioglioma is distinct from all other tumors; and (*d*) all tumors are distinct from normal tissue in cerebellum. It should be noted that because of the small size of the data set, we could not separate the data into two random groups for defining a discriminant function and then cross validating it. In addition, the misclassifications of the mixed tumor, the anaplastic ependymoma, and malignant teratoma are partially attributable to the small sample size and inability a priori to include these in the decision rule. Thus, the results in Table 4 are somewhat conservative.

TABLE 4: Effectiveness of the MR spectroscopy test for classification of the three major tumor types with NAA:Cho and Cr:Cho as predicting variables

Tumor Type	Sensitivity	Specificity	Positive Predictive Value	Negative Predictive Value
Astrocytoma	.91	.84	.77	.94
Ependymoma	.75	.92	.60	.96
Primitive neuroectodermal tumor	.82	.89	.82	.89

Note.—All tumors in Table 1 are included in this calculation. See text for detail.

Discussion

In a previous study of 25 brain tumors occurring in different regions in the brain (36), it was shown that benign astrocytomas and ependymomas were characterized by a decrease of NAA:Cho in comparison with normal tissue and an abnormal accumulation of lactate. Intrinsic malignant tumors were remarkable for an even lower NAA:Cho ratio but had no more lactate than was found in the benign tumors. In this study, the MR spectroscopy results for cerebellar tumors are consistent with the previous findings.

The in vivo MR spectroscopy shows that primitive neuroectodermal tumors have lower NAA:Cho than astrocytomas. This is consistent with a previous in vitro high-field MR spectroscopy study of extracts of pediatric cerebellar astrocytoma and primitive neuroectodermal tumor (53). The in vitro NAA:Cho for astrocytoma was a factor of 2.7 greater than that for primitive neuroectodermal tumor, in agreement with a factor of 3.7 found in vivo in this study. The in vitro result indicates that the two types of tumor have similar NAA levels, much lower

than that found in normal vermis. The choline level is higher in primitive neuroectodermal tumor than in astrocytoma. However, the Cr:Cho ratio for astrocytoma is 2.5 times that of primitive neuroectodermal tumor in vitro, whereas the in vivo ratio is not significantly different for the two tumor types. A part of this discrepancy may be caused by the lack of power to detect the difference in Cr:Cho of the two tumors in vivo.

The metabolite ratios observed in control cerebellum spectra are distinct from those of the tumor spectra. Proton MR spectroscopy of normal cerebellum have been reported (47, 54–57). The NAA:Cho in normal cerebellum is lower than that in normal cerebral hemispheres. Using values of concentration and relaxation times reported by Frahm et al (47), NAA:Cho in occipital white matter area can be calculated as 2.56 for a repetition time of 1600 milliseconds and an echo time of 135 milliseconds, and as 2.83 for a repetition time of 1500 milliseconds and an echo time of 270 milliseconds. Using metabolite T1, T2, and concentrations in cerebellum (47), peak area ratios NAA:Cho and Cr:Cho in adults can be calculated as 1.55 and 0.99, respectively, for a repetition time of 1600 milliseconds and an echo time of 135 milliseconds, which agrees with 1.59 and 1.15 in Table 2. For a repetition time of 1500 milliseconds and an echo time of 270 milliseconds, the calculated ratios are NAA:Cho of 1.37 and Cr:Cho of 0.68, compared with 1.33 and 1.09 in Table 2. There is a significant discrepancy in Cr:Cho ratio. Part of the difference in Cr:Cho could be attributable to age. However, even if the Cr:Cho ratio in control were lower than we found in this study, normal tissue still can be differentiated from tumors owing to its high NAA:Cho ratios.

The observed differences in the spectra of these tumors reflect the differences in their biochemistry and metabolism. Compared with normal tissue, NAA:Cho ratio was decreased in astrocytoma and ependymoma and even more so in primitive neuroectodermal tumor. The choline peak consists of several choline-containing compounds, including phosphoryl choline and glycerophosphoryl choline, which are involved in membrane synthesis and degradation. Therefore, higher choline levels were found in more aggressive tumor types. The main difference between astrocytomas and ependymomas was that the ependymomas had higher Cr:Cho ratios. Presently, we do not know the biochemical basis for this difference. NAA was not detected in the case of malignant teratoma, a germ cell tumor. This was consistent with the nonneuronal nature of this tumor.

It has been hypothesized that malignant tumors have a high metabolic rate (58). In one study, there was no direct correlation between hypermetabolism detected by positron emission tomography and lactate elevation detected by proton MR spectroscopy (28). Other reports found a correlation between glucose consumption rate and lactate levels for gliomas (25), but the areas with the most active metabolism did not have the highest lactate level (35). Elevated lactate suggests either oxygen deprivation or defects in the cancer cell respiration (59). Lactate is not necessarily detectable even under metabolic stress, because it may be washed away quickly and not accumulated in a sufficient amount. Because our data are normalized to choline levels, we will not be able to draw conclusions on the absolute level of lactate in these tumors. The mean value of Lac:Cho was higher in astrocytoma and ependymoma than in primitive neuroectodermal tumor, a more aggressive tumor type. The low Lac:Cho ratio in primitive neuroectodermal tumor is partly caused by the high choline levels in these tumors. However, in some primitive neuroectodermal tumors, the lactate was not seen in the spectra and some low-grade tumors clearly had elevated lactate level. Moreover, in a case of astrocytoma, which recurred later, the lactate level was not high.

Lipid signals were frequently observed in the in vivo spectra, especially with shorter echo times. Lactate measurements became difficult, because the CH_2 protons in the lipids also resonate at 1.3 ppm. Spectral editing techniques are needed to separate lactate and lipids signals. The presence of lipids also may obscure the NAA signal (52). It is possible that the lipid signal also contains diagnostic information and needs to be studied.

Data reported here were obtained before administration of a paramagnetic contrast agent. Two patients studied after gadopentetate dimeglumine injection were excluded from the data in "Results." One excluded case in this series was an astrocytoma that was strongly enhanced on T1-weighted MR. This tumor had NAA:Cho of 0.01 and Cr:Cho of 0.16, and it would fall into the primitive neuroectodermal tumor region in the Cr:Cho versus NAA:Cho scattergram. Be-

cause we did not measure the MR spectrum before injection of gadopentetate dimeglumine, we do not know whether the unusual spectral pattern in this tumor is caused by the contrast agent. The other tumor studied after contrast agent injection turned out to be an astrocytomaoligodendroglioma with leptomeningeal metastases (NAA:Cho = 0.44; Cr:Cho = 0.54). This tumor did not enhance after contrast agent injection. It would fall into the ependymoma region in Figure 1. The effects of the contrast agent on MR spectra have not been sufficiently documented. Specially designed studies may be needed to understand the effects of a contrast agent on MR spectroscopy. Experience of various MR centers suggest that this may or may not be important. Because the active component in gadopentetate dimeglumine is a negatively charged chelate, it has strongest effects on positively charged ions. Our MR spectroscopy studies of the metabolite solutions showed that the relaxavities of gadopentetate dimeglumine are larger on choline and myoinositol than NAA and lactate (Li et al, unpublished results, 1995). Conceivably, the effects observed in vivo will be important if the lesion is enhanced on MR, because the level of the contrast agent is higher. The effects will be less important if repetition time is long and echo time is short.

In this study, two types of pulse sequences were used for historic reasons. The data presented here were accumulated during several years. In the initial stage, STEAM was the only technique available, and an echo time of 270 milliseconds was used to avoid multiquantum effects on lactate. Later, spin-echo sequence with an echo time of 135 milliseconds was used for all studies for two reasons: (*a*) spin-echo sequence offers better signal detection sensitivity, and (*b*) we participated in a cooperative multicenter MR spectroscopy tumor study organized by Siemens, and a common protocol had to be used for all sites. There were potential problems for combining data acquired with these two sequences, such as effects of T2 relaxation, multiple quantum coherence, and diffusion and flow. For uncoupled spin systems such as $(CH_3)_3$ in choline and CH_3 in creatine and NAA, the expected major cause of differences in peak area ratios measured by these two sequences are caused by the different echo times used. For coupled spins such as CH and CH_3 in lactate, there are potentially multiple quantum effects if STEAM is used. However, these multiple quantum effects are not important for an echo time of 270 milliseconds. Therefore, the dominant effects responsible for difference in the Lac:Cho ratio also come from different echo time values used. However, Table 2 indicates that the mean values of ratios obtained with the two pulse sequences are very close to each other within each tumor type. A *t* test suggested that there was no significant difference in metabolite ratios based on sequence. Although the sample size for the *t* test is small, thus the power very limited, with a nonsignificant result, ratios from an echo time of 270 milliseconds could not be adjusted to what they would have been with an echo time of 135 milliseconds from a statistics point of view. Different tumor types often have different intensities on T2-weighted MR. Similarly, the T2 values for the metabolite also are likely to depend on the tumor type. Because T2 values for each metabolite in these tumors are not known, it is difficult to correct the effects of different echo times in these data. However, we may estimate the change of metabolite ratios attributable to different echo times by using the in vivo T2 values of the metabolites determined for normal tissue (47, 60) and astrocytomas (60). If we assume NAA:Cho and Cr:Cho ratios are 1.0 for an echo time of 135 milliseconds, these ratios are calculated in Table 5 using T2 values in different tissues for an echo time of 270 milliseconds. Therefore, if these estimates are good approximations, the ratios measured by STEAM sequence with echo time of 270 will vary by 3% to −24% for NAA:Cho, and −21% to −32% for Cr:Cho, compared with that obtained with spin-echo sequence with echo time of 135. Because most ependymomas were measured by this STEAM sequence and most astrocytomas and primitive neuroectodermal tumor were measured by this spin-echo sequence, the difference in Cr:Cho from ependymoma to astrocytoma and primitive neuroectodermal tumor would be larger if all data were acquired with the same sequence. Astrocytoma and primitive neuroectodermal tumor are differentiated by different NAA:Cho ratios. Table 5 suggests that for low-grade astrocytoma, the NAA:Cho ratio will not be sensitive to echo time. The situation for primitive neuroectodermal tumor is unknown but might be somewhat similar to high-grade astrocytoma, because both are malignant tumors with hypercellularity. If this is true, NAA:Cho will be lower by 24% if echo time is in-

TABLE 5: Calculated relative change in metabolite ratios when echo time is changed from 135 ms to 270 ms*, using T2 values from the literature

Tissue Type	T2, ms			Relative Change in Metabolite Ratios	
	Cho	Cr	NAA	NAA:Cho	Cr:Cho
Normal Brain†	378	229	413	1.03	0.79
Normal Cerebellum‡	410	190	300	0.87	0.68
Astrocytoma (grade 1–2)†	562	220	531	0.99	0.69
Astrocytoma (grade 3–4)†	410	216	226	0.76	0.74

* We assume the signal intensity is proportional to exp(−TE/T2).

† T2 values from Usenius et al (60).

‡ T2 values from Frahm et al (47).

creased from 135 milliseconds to 270 milliseconds. Therefore, if all tumors were studied with an echo time of 270 milliseconds, the discrimination between primitive neuroectodermal tumor and astrocytoma might be slightly better than found in this study. If, on the other hand, all data were collected using an echo time of 135 milliseconds, the sensitivities and specificities of the MR spectroscopy test for primitive neuroectodermal tumor and astrocytoma might have been slightly decreased. However, values in Table 2 do not suggest that NAA:Cho is sensitive to echo time for primitive neuroectodermal tumor.

Many types of brain tumors may occur in children, and some tumors are further divided into several grades. It is unlikely that one single spectroscopy index will differentiate between all tumors. However, different tumors are likely to exhibit different metabolic characteristics that are reflected in several metabolites. When the tumor spectra are characterized by several parameters, discriminant analysis is a convenient way to process the data and to use all the parameters optimally. Recently, Preul et al reported that linear discriminant analysis based on proton MR spectroscopy can be used to improve diagnosis for adult brain tumors (Preul MC et al, "Linear Discriminant Analysis. . ."). Six predicting variables (ratios of choline, creatine, NAA, alanine, lactate, and lipid to creatine in a control region) were used to distinguish the five most common adult supratentorial tumors, and in 99% of cases a correct result was obtained.

Recent in vitro MR spectroscopy study of pediatric brain tumor extracts showed that primitive neuroectodermal tumor has higher myoinositol, glycine, and taurine levels compared with astrocytoma (53). Moreover, glutamate level is higher in primitive neuroectodermal tumor than astrocytoma. These metabolites can be measured in vivo by proton MR spectroscopy with short echo times using current instruments. The accuracy of MR spectroscopy will improve when these metabolites are detected and quantified. Absolute quantitation of metabolites in the tumor also is likely to improve the accuracy of MR spectroscopy in the diagnoses of pediatric brain tumors.

Although CT and MR are the primary diagnostic imaging methods for initial diagnosis of brain tumors before surgery, MR spectroscopy may further increase the diagnostic accuracy and confidence. In many cases, the tumor type and degree of malignancy can be correctly predicted based on information obtained from MR and CT at the initial examination. Despite the many successes of diagnostic imaging, there also are many exceptions. Some common tumors have atypical appearances on MR and CT. Certain rare tumors mimic the appearance of more common tumors. The final diagnosis of a tumor still needs to be verified by microscopic pathologic examination of the biopsy specimen or the resected tumor tissue, even if surgical resection plays little role in the ultimate treatment. However, at times the pathology result is not completely correct or truly representative of the tumor, because the specimen was too small or obtained from the periphery of the tumor. A reliable initial diagnosis before a surgical procedure may help clinicians to choose the optimal treatment in the future. In certain cases, it also can reduce the MR examination time. For example, a staging spine MR study is needed for patients with primitive neuroectodermal tumor.

This examination can be saved if the tumor is an astrocytoma.

MR spectroscopy also may contain prognostic information. Although tumor histology is an important prognostic factor, parameters independent of tumor grade may have a crucial role in determining the growth rate of tumors. If prognosis can be established in an early stage, then therapy can be given more effectively with minimal side effects. In the case of primitive neuroectodermal tumor, adjuvant chemotherapy is recommended for poor risk patients in whom the outcome is predicted to be unfavorable based on degree of resection, metastases, and histology subtype. Because radiation therapy is harmful to the developing brain, several clinical trials have proposed reducing the dose in patients who are considered good risk on the basis of favorable prognostic factors. MR spectroscopy indices may be potentially useful in guiding the therapy.

References

1. Zimmerman RA, Bilaniuk LT, Rebsamen S. Magnetic resonance imaging of pediatric posterior fossa tumors. *Pediatr Neurosurg* 1992;18:58–64
2. Negendank W. Studies of human tumors by MRS: a review. *NMR Biomed* 1992;5:303–324
3. Zimmerman RA, Bottomley PA, Edelstein WA, et al. Proton imaging and phosphorus spectroscopy in a malignant glioma. *AJNR Am J Neuroradiol* 1985;6:109–110
4. Oberhaensli RD, Hilton-Jones D, Bore PJ, Hands LJ, Rampling RP, Radda GK. Biochemical investigation of human tumors in vivo with phosphorus-31 magnetic resonance spectroscopy. *Lancet* 1986;2:8–11
5. Naruse S, Horikawa Y, Tanaka C, et al. Evaluation of the effects of photoradiation therapy on brain tumors with in vivo P-31 MR spectroscopy. *Radiology* 1986;160:827–830
6. Arnold DL, Shoubridge EA, Feindel W, Villemure JG. Metabolic changes in cerebral gliomas within hours of treatment with intra-arterial BCNU demonstrated by phosphorus magnetic resonance spectroscopy. *Can J Neurol Sci* 1987;14:570–575
7. Segebarth CM, Baleriaux DF, Arnold DL, Luyten PR, den Hollander JA. MR image-guided P-31 MR spectroscopy in the evaluation of brain tumor treatment. *Radiology* 1987;165:215–219
8. Heindel W, Bunke J, Glathe S, Steinbrich W, Mollevanger L. Combined 1H-MR imaging and localized 31P-spectroscopy of intracranial tumors in 43 patients. *J Comput Assist Tomogr* 1988;12:907–916
9. Thomsen C, Jensen KE, Achten E, Henriksen O. In vivo magnetic resonance imaging and 31P spectroscopy of large human brain tumours at 1.5 tesla. *Acta Radiol* 1988;29:77–82
10. den Hollander JA, Luyten PR, Marien AJ, et al. Potentials of quantitative image-localized human 31P nuclear magnetic resonance spectroscopy in the clinical evaluation of intracranial tumors. *Magn Reson Q* 1989;5:152–168
11. Glickson JD. Clinical NMR spectroscopy of tumors: current status and future directions. *Invest Radiol* 1989;24:1011–1016
12. Bruhn B, Frahm J, Gyngell ML, et al. Noninvasive differentiation of tumors with use of localized H-1 MR spectroscopy in vivo: initial experience in patients with cerebral tumors. *Radiology* 1989;172:541–548
13. Gill SS, Small RK, Thomas DG, et al. Brain metabolites as 1H NMR markers of neuronal and glial disorders. *NMR Biomed* 1989;2:196–200
14. Ross BD, Tropp J, Derby KA, et al. Metabolic response of glioblastoma to adoptive immunotherapy: detection by phosphorus MR spectroscopy. *J Comput Assist Tomogr* 1989;13:189–193
15. Arnold DL, Shoubridge EA, Emrich J, Feindel W, Villemure JG. Early metabolic changes following chemotherapy of human gliomas in vivo demonstrated by phosphorus magnetic resonance spectroscopy. *Invest Radiol* 1989;24:958–961
16. Hubesch B, Marinier DS, Hetherington HP, Twieg DB, Weiner MW. Clinical MRS studies of the brain. *Invest Radiol* 1989;24:1039–1042
17. Langkowski JH, Wieland J, Bomsdorf H, et al. Pre-operative localized in vivo proton spectroscopy in cerebral tumors at 4.0 tesla-first results. *Magn Reson Imaging* 1989;7:547–555
18. Weiner MW, Heterington H, Hubesch B, et al. Clinical magnetic resonance spectroscopy of brain, heart, liver, kidney, and cancer: a quantitative approach. *NMR Biomed* 1989;2:290–297
19. Segebarth CM, Baleriaux DF, de Beer R, et al. 1H image-guided localized 31P MR spectroscopy of human brain: quantitative analysis of 31P MR spectra measured on volunteers and on intracranial tumor patients. *Magn Reson Med* 1989;11:349–366
20. Cadoux-Hudson TA, Blackledge MJ, Rajagopalan B, Taylor DJ, Radda GK. Human primary brain tumor metabolism in vivo: a phosphorus magnetic resonance spectroscopy study. *Br J Cancer* 1989;60:430–436
21. Heiss WD, Heindel W, Herholz K, et al. Positron emission tomography of fluorine-18-deoxyglucose and image-guided phosphorus-31 magnetic resonance spectroscopy in brain tumors. *J Nucl Med* 1990;31:302–310
22. Segebarth CM, Baleriaux DF, Luyten PR, den Hollander JA. Detection of metabolic heterogeneity of human intracranial tumors in vivo by 1H NMR spectroscopic imaging. *Magn Reson Med* 1990;13:62–76
23. Gill SS, Thomas DGT, Van Bruggen N, et al. Proton MR spectroscopy of intracranial tumours: in vivo and in vitro studies. *J Comput Assist Tomogr* 1990;14:497–504
24. Sutton LN, Lenkinski RE, Cohen BH, Packer RJ, Zimmerman RA. Localized 31P magnetic resonance spectroscopy of large pediatric brain tumors. *J Neurosurg* 1990;72:65–70
25. Luyten PR, Marien AJH, Heindel W, et al. Metabolic imaging of patients with intracranial tumors: H-1 MR spectroscopic imaging and PET. *Radiology* 1990;176:791–799
26. Hubesch B, Sappey-Marinier D, Roth K, Meyerhoff DJ, Matson GB, Weiner MW. P-31 MR spectroscopy of normal human brain and brain tumors. *Radiology* 1990;174:401–409
27. Sostman HD, Charles HC. Noninvasive differentiation of tumors with use of localized H-1 spectroscopy in vivo: initial experience in patients with cerebral tumors. *Invest Radiol* 1990;25:1047–1050
28. Alger JR, Frank JA, Bizzi A, et al. Metabolism of human gliomas: assessment with H-1 MR spectroscopy and F-18 fluorodeoxyglucose PET. *Radiology* 1990;177:633–641
29. Demaerel P, Johannik K, Van Hecke P, et al. Localized 1H NMR spectroscopy in fifty cases of newly diagnosed intracranial tumors. *J Comp Assist Tomogr* 1991;15:67–76
30. Arnold DL, Emrich JF, Shoubridge EA, Villemure JG, Feindel W. Characterization of astrocytomas, meningiomas, and pituitary adenomas by phosphorus magnetic resonance spectroscopy. *J Neurosurg* 1991;74:447–453

31. Henrikson O, Wieslander S, Gjerris F, Jensen KM. In vivo 1H-spectroscopy of human intracranial tumors at 1.5 tesla. Pleliminary experience at a clinical installation. *Acta Radiologica* 1991; 32:95–99
32. Taylor JS, Vigneron DB, Murphy-Boesch J, et al. Free magnesium levels in normal human brain and brain tumors: 31P chemical-shift imaging measurements at 1.5 T. *Proc Natl Acad Sci USA* 1991;88:6810–6814
33. Frahm J, Bruhn H, Hanicke W, Merboldt K-D, Mursch K, Markakis E. Localized proton NMR spectroscopy of brain tumors using short-echo time STEAM sequences. *J Comput Assist Tomogr* 1991;15:915–922
34. Kugel H, Heindel W, Ernestus RI, Bunke J, du Mesnil R, Friedmann G. Human brain tumors: spectral patterns detected with localized H-1 MR spectroscopy. *Radiology* 1992;183:701–709
35. Herholz K, Heindel W, Luyten PR, et al. In vivo imaging of glucose consumption and lactate concentration in human gliomas. *Ann Neurol* 1992;31:319–327
36. Sutton LN, Wang Z, Gusnard D, et al. Proton magnetic resonance spectroscopy of pediatric brain tumors. *Neurosurgery* 1992;31: 195–202
37. Fulham MJ, Bizzi A, Dietz MJ, et al. Mapping of brain tumor metabolites with proton MR spectroscopic imaging: clinical relevance. *Radiology* 1992;185:675–686
38. Barker PB, Glickson JD, Bryan RN. In vivo nuclear magnetic resonance spectroscopy of human brain tumors. *Top Magn Reson Imaging* 1993;5:32–45
39. Ott D, Hennig J, Ernst T. Human brain tumors: assessment with in vivo proton MR spectroscopy. *Radiology* 1993;186:745–752
40. Tzika AA, Vigneron DB, Ball WSJ, Dunn RS, Kirks DR. Localized proton MR spectroscopy of the brain in children. *J Magn Reson Imaging* 1993;3:719–729
41. Baka JJ, Patel SC, Roebuck JR, Hearshen DO. Predominantly extraaxial astroblastoma: imaging and proton MR spectroscopy features. *AJNR Am J Neuroradiol* 1993;14:946–950
42. Jungling FD, Wakhloo AK, Hennig J. In vivo proton spectroscopy of meningioma after preoperative embolization. *Magn Reson Med* 1993;30:155–160
43. Madison MT, Hall WA, Latchaw RE, Loes DJ. Radiologic diagnosis, staging, and follow-up of adult central nervous system primary malignant glioma. *Radiol Clin North Am* 1994;32:183–196
44. Frahm J, Merboldt KD, Hanicke W. Localized proton spectroscopy using stimulated echoes. *J Magn Reson* 1987;72:502–508
45. Bottomley PA. Spatial localization in NMR spectroscopy in vivo. *Ann NY Acad Sci* 1987; 508:333–348
46. Klose U. In vivo proton spectroscopy in presence of eddy currents. *Magn Reson Med* 1990;14:26–30
47. Frahm J, Bruhn H, Gyngell ML, Merboldt KD, Hanicke W, Sauter R. Localized proton NMR spectroscopy in different regions of the human brain in vivo: relaxation times and concentrations of cerebral metabolites. *Magn Reson Med* 1989;11:47–63
48. Ernst RR. Sensitivity enhancement in NMR spectroscopy. *Adv Magn Reson* 1966;2:1–135
49. de Beer R, van Ormondt D. Quantitative data analysis in MRS: where to go? *Eurospin Annual* 1994;37–48
50. Mehta CR, Patel NR. A network algorithm for performing Fisher's exact test in r x c contingency tables. *J Am Stat Assoc* 1983;78: 427–434
51. Klecka WR. *Discriminant Analysis*. Beverly Hills, Calif: Sage Publications; 1980;1
52. Kuesel A, Sutherland G, Halliday W, Smith I. 1H MRS of high grade astrocytomas: mobile lipid accumulation in necrotic tissue. *NMR Biomed* 1994;7:149–155
53. Sutton LN, Wehrli SL, Gennarelli L, et al. High-resolution 1H-magnetic resonance spectroscopy of pediatric posterior fossa tumors in vitro. *J Neurosurg* 1994;81:443–448
54. Huppi PS, Posse S, Lazeyras F, Burri R, Bossi E, Herschkowitz N. Magnetic resonance in preterm and term newborns: 1H-spectroscopy in developing human brain. *Pediatric Res* 1991;30:574–578
55. Hennig J, Pfister H, Ernst T, Ott D. Direct absolute quantitation of metabolites in the human brain with in vivo localized proton spectroscopy. *NMR Biomed* 1992;5:193–199
56. Michaelis T, Merboldt K-D, Bruhn H, Hanicke W, Frahm J. Absolute concentration of metabolites in the adult human brain in vivo: quantification of localized proton MR spectra. *Neuroradiology* 1993;187:219–227
57. Fulham MJ, Dietz MJ, Duyn JH, Shih HH-L, Alger JR, Di Chiro G. Transsynaptic reduction in N-acetyl-aspartate in cerebellar Diaschisis: a proton MR spectroscopic imaging study. *J Comput Assist Tomogr* 1994;18:697–704
58. Di Chiro G, DeLaPaz RL, Brooks RA, et al. Glucose utilization of cerebral gliomas measured by [18F] flurodeoxyglucose and positron emission tomography. *Neurology* 1982;32:1323–1329
59. Warburg O. On the origin of cancer cells. *Science* 1956;123:309–314
60. Usenius J-PR, Kauppinen RA, Vainio PA, et al. Quantitative metabolite patterns of human brain tumors: detection by 1H NMR spectroscopy in vivo and in vitro. *J Comput Assist Tomogr* 1994; 18:705–713